


Diffusion kurtosis imaging of the liver at 3 Tesla: in vivo comparison to standard diffusion-weighted imaging

Johannes Budjan^{1,*}, Elke A Sauter^{1,*}, Frank G Zoellner²,
Andreas Lemke², Jens Wambsganss¹, Stefan O Schoenberg¹
and Ulrike I Attenberger¹

Acta Radiologica
0(0) 1–8
© The Foundation Acta Radiologica
2017
Reprints and permissions:
sagepub.co.uk/journalsPermissions.nav
DOI: 10.1177/0284185117706608
journals.sagepub.com/home/acr


Abstract

Background: Functional techniques like diffusion-weighted imaging (DWI) are gaining more and more importance in liver magnetic resonance imaging (MRI). Diffusion kurtosis imaging (DKI) is an advanced technique that might help to overcome current limitations of DWI.

Purpose: To evaluate DKI for the differentiation of hepatic lesions in comparison to conventional DWI at 3 Tesla.

Material and Methods: Fifty-six consecutive patients were examined using a routine abdominal MR protocol at 3 Tesla which included DWI with b-values of 50, 400, 800, and 1000 s/mm². Apparent diffusion coefficient maps were calculated applying a standard mono-exponential fit, while a non-Gaussian kurtosis fit was used to obtain DKI maps. ADC as well as Kurtosis-corrected diffusion (*D*) values were quantified by region of interest analysis and compared between lesions.

Results: Sixty-eight hepatic lesions (hepatocellular carcinoma [HCC] [*n* = 25]; hepatic adenoma [*n* = 4], cysts [*n* = 18]; hepatic hemangioma [HH] [*n* = 18]; and focal nodular hyperplasia [*n* = 3]) were identified. Differentiation of malignant and benign lesions was possible based on both DWI ADC as well as DKI *D*-values (*P* values were in the range of 0.04 to < 0.0001).

Conclusion: In vivo abdominal DKI calculated using standard b-values is feasible and enables quantitative differentiation between malignant and benign liver lesions. Assessment of conventional ADC values leads to similar results when using b-values below 1000 s/mm² for DKI calculation.

Keywords

Magnetic resonance imaging (MRI), diffusion-weighted imaging (DWI), diffusion kurtosis imaging (DKI), liver, focal liver lesions, 3 Tesla

Date received: 1 June 2016; accepted: 21 March 2017

Introduction

Diffusion describes the random Brownian motion of gaseous or liquid molecules. Signal changes on diffusion-weighted imaging (DWI) represent alterations in the microscopic mobility of water in tissues. In a homogeneous medium, diffusion is described as having Gaussian behavior. However, in general, the diffusion of water in living tissues is restricted by interactions with other molecules and cell membranes and is therefore thought to display non-Gaussian diffusion properties. The choice of b-values in conventional DWI influences the apparent diffusion coefficients (ADC)

¹Department of Clinical Radiology and Nuclear Medicine, University Medical Center Mannheim, Medical Faculty Mannheim, Heidelberg University, Mannheim, Germany

²Computer Assisted Clinical Medicine, Medical Faculty Mannheim, Heidelberg University, Germany

*Equal contributors.

Corresponding author:

Johannes Budjan, Department of Clinical Radiology and Nuclear Medicine, University Medical Center Mannheim, Medical Faculty Mannheim, Heidelberg University, Theodor-Kutzer-Ufer 1-3, 68167 Mannheim, Germany.
Email: johannes.budjan@umm.de

obtained. Diffusion kurtosis imaging (DKI) has been proposed as a novel imaging technique to help overcome this limitation. DKI as a diffusion model was introduced by Jensen in 2005 (1) to account for the non-Gaussian diffusion properties of water in complex structures. DKI enables acquisition of dimensionless measurements reflecting the degree of diffusion restriction (1–3). Results obtained with DKI models may thus better reflect diffusion properties in tissue.

DKI has been investigated in the central nervous system to evaluate conditions such as malignancy, degenerative processes, and stroke (4–7), and has recently been applied to imaging of prostate cancer (8) and the ex vivo assessment of hepatocellular carcinoma (9,10). For prostate imaging, DKI showed a higher sensitivity in the differentiation of both normal from cancerous areas as well as low- from high-grade carcinomas (8). In hepatocellular carcinoma, a non-Gaussian behavior of diffusion was found ex vivo, with Kurtosis corrected diffusion coefficients being statistically significantly higher than conventional ADC values (10). In those applications, DKI protocols typically included additional ultra-high b-values for DKI calculations. However, the number of b-values acquired in clinical protocols is typically limited to 3–5, especially as high b-value DWI requires averaging to receive sufficient signal-to-noise ratio (SNR) on clinical magnetic resonance (MR) scanners. Particularly in severely ill patients, the necessary increase in examination time needed for additional b-value acquisition becomes the limiting factor for including DKI as described in ex vivo studies in clinical routine protocols. As shown for applications in the imaging of pancreatic lesions, DKI derived from clinical standard b-values can deliver additional information beyond calculations based on mono-exponential fit (11). To date, no previous studies have investigated the feasibility of DKI for the differentiation of hepatic lesions in vivo. The aim of the study was to evaluate the diagnostic performance of clinical standard b-value based DKI in comparison to standard ADC for the differentiation of benign and malignant focal hepatic lesions.

Material and Methods

Patients

Following Institutional Review Board approval, 56 consecutive patients (38 men; mean age, 57 years; age range, 21–86 years) were included in this retrospective study. Patients were referred for liver MRI for different indications including cancer staging, characterization of known focal lesions and follow-up examinations.

MR imaging

Magnetic resonance imaging (MRI) examination was performed according to our institutional standard operation procedure at a 3 Tesla whole-body MR scanner (Magnetom Skyra, Siemens Healthcare, Erlangen, Germany). Depending on the clinical indication for the study, an extracellular, non-specific (n=20 patients, gadoterate meglumine [Dotarem®, Guerbet, Roissy, France]) or a liver-specific (n=36, gadoxetic acid [Primovist®, Bayer Vital GmbH, Leverkusen, Germany]) contrast agent was used. The imaging protocol included T1-weighted (T1W) axial pre-contrast VIBE, T2-weighted (T2W) coronal and axial HASTE with and without fat suppression and post-contrast multi-phase T1W VIBE sequences. In patients receiving the extracellular contrast agent (ECCA group), DWI sequences were acquired prior to contrast injection. In patients receiving the hepatocyte-specific contrast agent (HSCA group), DWI was acquired starting 3 min post contrast injection. DWI was performed using a single-shot echo-planar sequence with b-values of 50, 400, 800, and 1000 s/mm². Sequence parameters were: TE/TR, 75/7800; averages, 1 for b=50 s/mm² to 5 for b=1000 s/mm²; acquisition matrix, 192 × 140; field of view, 340 × 240; flip angle, 90°; parallel acquisition factor, GRAPPA 2; bandwidth, 1644 Hz/pixel; slice thickness, 4 mm; spectral fat suppression.

DKI post-processing

UMM Diffusion (Version 0.2.3), an open source plugin for OsiriX (Version 5.6, OsiriX Foundation, Geneva, Switzerland), was used to generate ADC and DKI maps (12,13) based on the four acquired b-values. A standard mono-exponential fit was used to calculate ADC, and a non-Gaussian kurtosis fit was used to calculate the DKI values K, a measure of excess kurtosis of diffusion, and D, a corrected diffusion coefficient accounting for this non-Gaussian behavior. To generate DKI maps, the following equation was fit pixel-wise to the image data (2):

$$\ln\left(\frac{S(b)}{S(b_0)}\right) = -bD + \frac{1}{6}b^2D^2K$$

where S(b) represents the images acquired with different b-values (diffusion weightings) and S(b₀) is the signal of the unweighted image.

Image analysis

Image analysis was performed by two radiologists with eight and four years of experience in abdominal MRI, respectively. The readers had access to all available image data to identify focal liver lesions. For every

lesion that was identified, a region of interest (ROI) approach was used to further analyze ADC and DKI maps. ROIs were placed in the lesions and directly copied from ADC to DKI maps. Care was taken to exclude vessels and bile ducts when placing the ROIs. To reduce the influence of signal noise while minimizing partial volume effects, ROIs were placed on three consecutive slices including the lesion center. Mean ADC, mean corrected diffusion (D), and mean kurtosis value (K) were calculated. For final lesion characterization and classification, all available clinical information (including histology after biopsy or resection) and/or previous and follow-up examinations was taken into account. Lesions with homogenous low signal on T1W and very high signal on T2W sequences without changes in T1 signal intensity after injection of the contrast agent and without septations or wall irregularities were classified as cysts.

Statistical analysis

Statistical analyses were performed using SAS 9.4 (SAS Institute, Cary, NC, USA) and StatXact (Cytel Studio, Cambridge, MA, USA). DWI and DKI parameters were compared using t-tests. In case of multiple testing, Bonferroni correction was performed. Twofold

unbalanced ANOVA for the lesion groups and contrast media was performed. A classification of malignancy in terms of ADC and diffusion values are given and compared to the histologic findings. Based on that a sensitivity analysis and a ROC curve analysis is presented. All values are reported as mean \pm standard deviation. A P value <0.05 was considered statistically significant.

Results

The Kurtosis fitting model as well as the standard mono-exponential fit could be applied and DKI and ADC maps were generated successfully in all cases (Fig. 1). In the ECCA group, a total of 23 focal liver lesions was identified, consisting of nine cysts, eight hepatocellular carcinomas (HCC), and six hepatic hemangiomas (HH). Forty-five lesions in total were found in the HSCA group, consisting of four hepatic adenomas (HA), three focal nodular hyperplasias (FNH), 12 HHs, 17 HCCs, and nine cysts. For HCCs, all lesions except for two were confirmed by histology after biopsy ($n = 22$) or resection ($n = 1$). In two cases, histology was not available; however, both patients underwent additional computed tomography (CT) or contrast-enhanced sonography, in which the lesions were also found to be highly suspicious of HCC. For HH, two

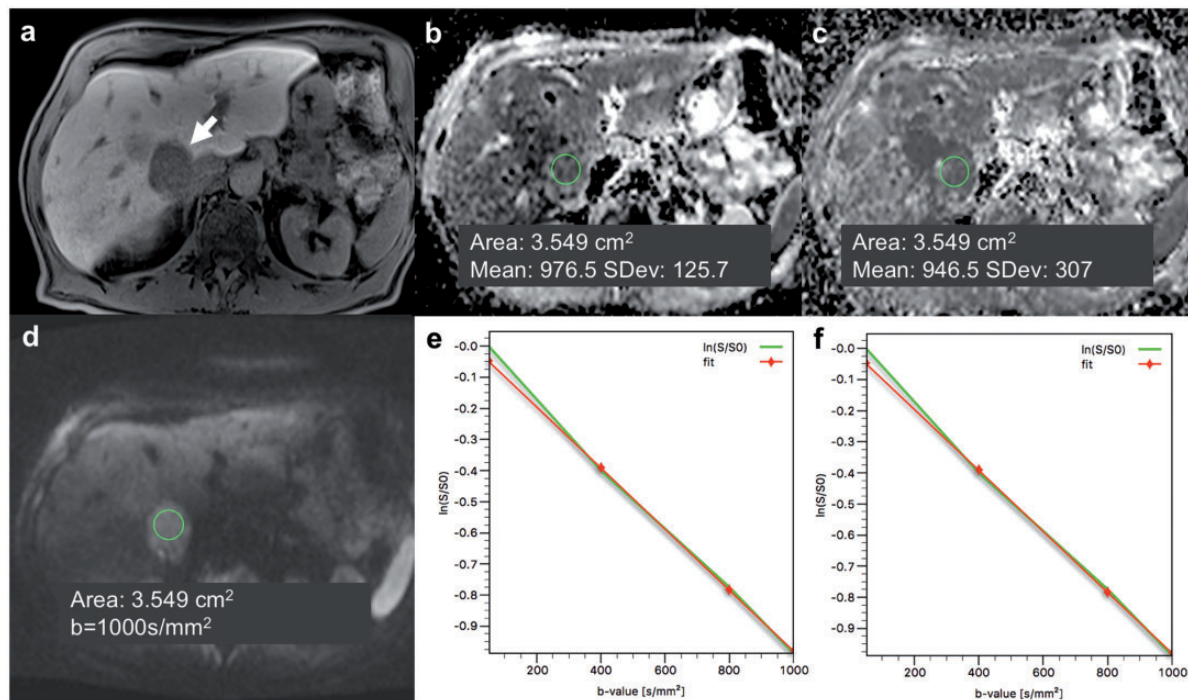


Fig. 1. Example of a histologically proven HCC in a 76-year-old patient with liver cirrhosis. (a) A T1W axial image in the hepatobiliary phase 20 min post injection. The lesion shows both low ADC values ((b) ADC map) as well as low D values ((c) DKI map). The maps were calculated using b-values of 50, 400, 800, and 1000 s/mm² (b = 1000 s/mm² shown in (d)). Both fitting models result in similar curves: (e) mono-exponential fitting curve; (f) DKI fitting curve.

lesions were confirmed by histology after resection; mean follow-up time of the remaining HH was 14 months. One FNH was confirmed by histology after resection; mean follow-up time for remaining FNH was 48 months. Mean follow-up for HA was 32 months. In total, 68 hepatic lesions were included, of which 25 were malignant (HCC) and 43 benign (HH, HA, FNH, and cysts).

ADC analysis

In the analysis of ADC values, hepatic cysts showed the highest ADC values (mean ADC for ECCA group $2.916 \pm 0.372 * 10^{-3} \text{ mm/s}^2$, HSCA group $2.648 \pm 0.420 * 10^{-3} \text{ mm/s}^2$), while HCCs featured the lowest ADC values of all lesions for both contrast agent groups (ECCA group $0.922 \pm 0.220 * 10^{-3} \text{ mm/s}^2$, HSCA group $0.789 \pm 0.191 * 10^{-3} \text{ mm/s}^2$). HH were found to show intermediate ADC values (ECCA group $1.921 \pm 0.527 * 10^{-3} \text{ mm/s}^2$, HSCA group $1.698 \pm 0.437 * 10^{-3} \text{ mm/s}^2$). Mean ADC for HA (HSCA group $1.328 \pm 0.224 \text{ mm/s}^2$) was lower than HH, but higher than HCC.

In the comparison of mean ADC values in both contrast agent groups, HCC showed statistically significant differences in comparison to cysts ($P < 0.0001$), HH ($P < 0.0001$), and HA ($P = 0.01$), while no statistically significant difference was found in the comparison to FNH ($P = 0.16$).

Table 1 and Fig. 2 give an overview over ADC values for the different lesion types.

Mean ADC was statistically significantly lower for malignant lesions compared to benign lesions ($0.830 \pm 0.210 * 10^{-3} \text{ mm/s}^2$ versus $2.110 \pm 0.730 * 10^{-3} \text{ mm/s}^2$, $P < 0.0001$).

The variance between the lesion groups and the treatment factors was statistically significant ($P < 0.0001$ and $P = 0.04$, respectively). A leading opposite influence by HCC lesions compared to HH and cysts and minor influence of the contrast process used was found (group effects for HCC = -0.842 ; HH = 0.096 ; and cysts = 1.073 ; treatment effects HSCA = -0.076 and ECCA = 0.126 considering interaction). Reduction of the model without interaction lead to slightly altered estimated group and treatment effects: HCC = -0.853 ; HH = 0.088 ; and cysts = 1.098 ; HSCA = -0.168 and ECCA = 0.278 , respectively.

Kurtosis analysis

In the analysis of the kurtosis corrected diffusion coefficient D, hepatic cysts showed the highest D values (mean D $4.223 \pm 1.553 * 10^{-3} \text{ mm/s}^2$ in the ECCA group, $3.201 \pm 1.610 * 10^{-3} \text{ mm/s}^2$ in the HSCA group) of all focal liver lesions in both contrast agent groups. As with ADC values, HCCs featured the lowest D values of all focal liver lesions in both contrast agent groups ($0.970 \pm 0.467 * 10^{-3} \text{ mm/s}^2$ in the ECCA group, $0.923 \pm 0.391 * 10^{-3} \text{ mm/s}^2$ in the HSCA group). In the comparison of mean D values in both contrast agent groups, HCC showed statistically significant differences in comparison to cysts ($P < 0.0001$), HH ($P < 0.0001$), and HA ($P = 0.04$), while no statistically significant difference was found in the comparison to FNH ($P = 0.25$).

Table 2 and Fig. 2 give an overview over D values in different lesions. Mean D was statistically significantly lower for malignant lesions compared to benign lesions ($0.94 \pm 0.4 * 10^{-3} \text{ mm/s}^2$ versus $2.730 \pm 1.5 * 10^{-3} \text{ mm/s}^2$, $P < 0.0001$).

Table 1. Overview over ADC values in different lesions.

			Lesions (n (patients))	Mean \pm SD	Median	Min–Max [Range]
All			45 (36)	1.473 ± 0.766	1.329	0.293–3.226 [2.933]
HSCA group	Adenoma		4 (4)	1.328 ± 0.224	1.278	1.112–1.643 [0.531]
	FNH		3 (3)	1.115 ± 0.262	0.973	0.955–1.417 [0.462]
	HH		12 (12)	1.698 ± 0.437	1.582	1.329–2.641 [1.312]
	HCC		17 (14)	0.789 ± 0.191	0.789	0.293–1.089 [0.796]
	Cyst		9 (9)	2.648 ± 0.420	2.580	2.120–3.226 [1.106]
All			23 (20)	1.963 ± 0.946	2.080	0.612–3.435 [2.823]
ECCA group	HH		6 (6)	1.921 ± 0.527	1.946	1.129–2.726 [1.597]
	HCC		8 (6)	0.922 ± 0.220	0.8995	0.612–1.355 [0.7427]
	Cyst		9 (9)	2.916 ± 0.372	2.966	2.425–3.435 [1.010]

All values except number of lesions are given in $* 10^{-3} \text{ mm/s}^2$.

Sequence acquisition was performed after contrast administration in the HSCA group and prior contrast administration in the ECCA group.

ECCA, extracellular contrast agent; FNH, focal nodular hyperplasia; HCC, hepatocellular carcinoma; HH, hepatic hemangioma; HSCA, hepatocyte specific contrast agent; SD, standard deviation.

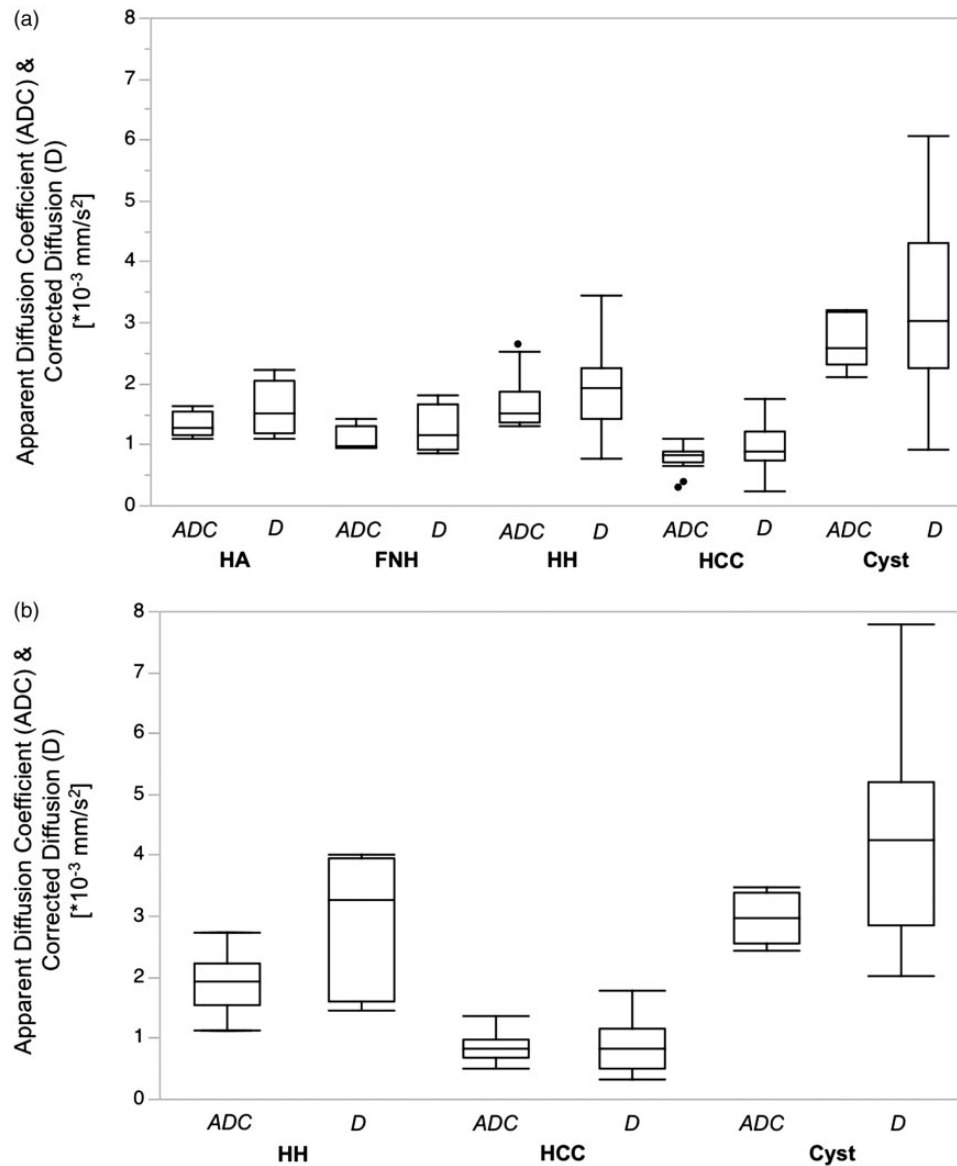


Fig. 2. ADC and D values for different hepatic lesions in different contrast agent groups for HSCA (a) and ECCA (b) group (FNH, focal nodular hyperplasia; HH, hepatic hemangioma; HCC, hepatocellular carcinoma; HSCA, hepatocyte specific contrast agent; ECCA, extracellular contrast agent). Note: Sequence acquisition was performed after contrast administration in the HSCA group and prior contrast administration in the ECCA group.

In the analysis of K values, no statistically significant differences were found between cysts (mean K values ECCA group = 0.221, HSCA group = -0.843), HH (ECCA = 0.573, HSCA = -0.439), HCC (ECCA = -2.859, HSCA = -0.843), FNH (HSCA = 0.472) and HA (HSCA = 0.415) for both contrast agent groups.

The variance between the lesion groups and the treatment factors was statistically significant ($P < 0.0001$ and $P = 0.02$, respectively). A leading opposite influence by HCC lesions compared to HH and cysts and an influence of the contrast process used was found (group effects for HCC = -1.16;

HH = 0.12; and cysts = 1.50; treatment effects HSCA = -0.246 and ECCA = 0.407 considering interaction). Reduction of the model without interaction lead to slightly altered estimations of group and some sharper treatment effects: HCC = -1.20; HH = 0.09; and cysts = 1.58; HSCA = -0.374 and ECCA = 0.619, respectively.

Diagnostic performance of ADC and DKI

Based on the descriptive analysis, a threshold value of $1.21 \times 10^{-3} \text{ mm/s}^2$ in ADC and of $1.36 \times 10^{-3} \text{ mm/s}^2$ in D

Table 2. Overview over D values in different lesions.

		Lesions (n (patients))	Mean \pm SD	Median	Min–Max [Range]
	All	45 (36)	1.718 \pm 1.172	1.451	0.224–6.060 [5.836]
HSCA group	HA	4 (4)	1.592 \pm 0.463	1.522	1.107–2.217 [1.114]
	FNH	3 (3)	1.334 \pm 0.431	1.193	0.9935–1.818 [0.825]
	HH	12 (12)	1.870 \pm 0.669	1.935	0.783–3.456 [2.673]
	HCC	17 (14)	0.923 \pm 0.391	0.898	0.224–1.758 [1.534]
	Cyst	9 (9)	3.201 \pm 1.610	3.016	0.911–6.060 [5.149]
	All	23 (20)	2.755 \pm 1.812	2.864	0.502–7.788 [7.286]
ECCA group	HH	6 (6)	2.930 \pm 1.131	3.261	1.459–4.005 [2.546]
	HCC	8 (6)	0.970 \pm 0.467	0.854	0.502–1.772 [1.272]
	Cyst	9 (9)	4.223 \pm 1.553	4.077	2.808–7.788 [4.981]

All values except number of lesions are given in $\times 10^{-3}$ mm/s².

Sequence acquisition was performed after contrast administration in the HSCA group and prior contrast administration in the ECCA group.

ECCA, extracellular contrast agent; FNH, focal nodular hyperplasia; HA, hepatic adenoma; HCC, hepatocellular carcinoma; HH, hepatic hemangioma; HSCA, hepatocyte specific contrast agent; SD, standard deviation.

value was assumed. Five classes of malignancies were grouped around these values (Table 3). Sensitivity, specificity, positive predictive value (PPV), and negative predictive value (NPV) for ADC were 85.7%, 97.5%, 96.0%, and 90.7%, respectively. For D, sensitivity, specificity, PPV, and NPV were 75.0%, 90.0%, 84.0%, and 83.7%, respectively. In the ROC analysis, the area under curve (AUC) was 0.9149 for ADC and 0.9847 for D (Fig. 3).

Discussion

Our results demonstrate that D, the corrected diffusion coefficient, derived from a standard clinical DWI protocol allows a differentiation of focal benign and malignant liver lesions. D values derived from a clinical DWI protocol including b-values up to 1000 s/mm² showed a separation effect that was comparable to the conventional ADC values. The potential value of DKI for focal liver lesion differentiation is underlined by a recent study, in which DKI allowed for an ex vivo differentiation between non-, partially and completely necrotic hepatocellular carcinomas (10). In vivo, however, studies specifically investigating the value of DKI for the differentiation of focal liver lesions have not yet been performed. In contrast to ex vivo liver imaging, in vivo MRI is influenced by respiratory motion artifacts, pulsation artifacts of the liver vessels, and particularly a limited scan time. While Rosenkrantz et al. (14) suggest higher b-values than 1000 s/mm², the practicability of such an approach is limited by low SNR at clinical scanners (15). Especially for critically ill patients, the additional scanning time needed particularly for the acquisition of ultra-high b-value DWI will

Table 3. Classification of malignancy in terms of ADC and D values.

Class		Limits: ADC	Limits: D
1	Definitely benign	>1.4	>1.77
2	Probably benign	1.275–1.4	1.77–1.42
3	Possibly malignant	1.15–1.275	1.42–1.10
4	Probably malignant	1.15–0.9	1.10–0.77
5	Definitely malignant	<0.9	<0.77

Left open intervals; all values are given in $\times 10^{-3}$ mm/s².

often not be tolerated, resulting in premature termination of the examination or reduction of image quality because of motion artifacts.

Thus, the focus of this work was the evaluation of DKI analysis based on a clinical feasible and routinely used protocol without any additional acquisition time and utilizing an in-house built software plug-in in a ready-to-use approach.

While conventional DWI has been proven to be a useful tool for the evaluation of abdominal lesions, its limitations are well-known including non-standardization of protocols, subsequent variability in reported ADC values, and ADC value dependence on field strength, vendor, and variations in calculation techniques (mono versus bi-exponential) (16). A recent study compared DKI and conventional DWI in the assessment of therapeutic effects in HCC treatment (9). In this study, DKI was found to provide a higher diagnostic performance in the detection of viable HCCs after therapy than conventional DWI. The authors postulate that DKI might be less influenced by

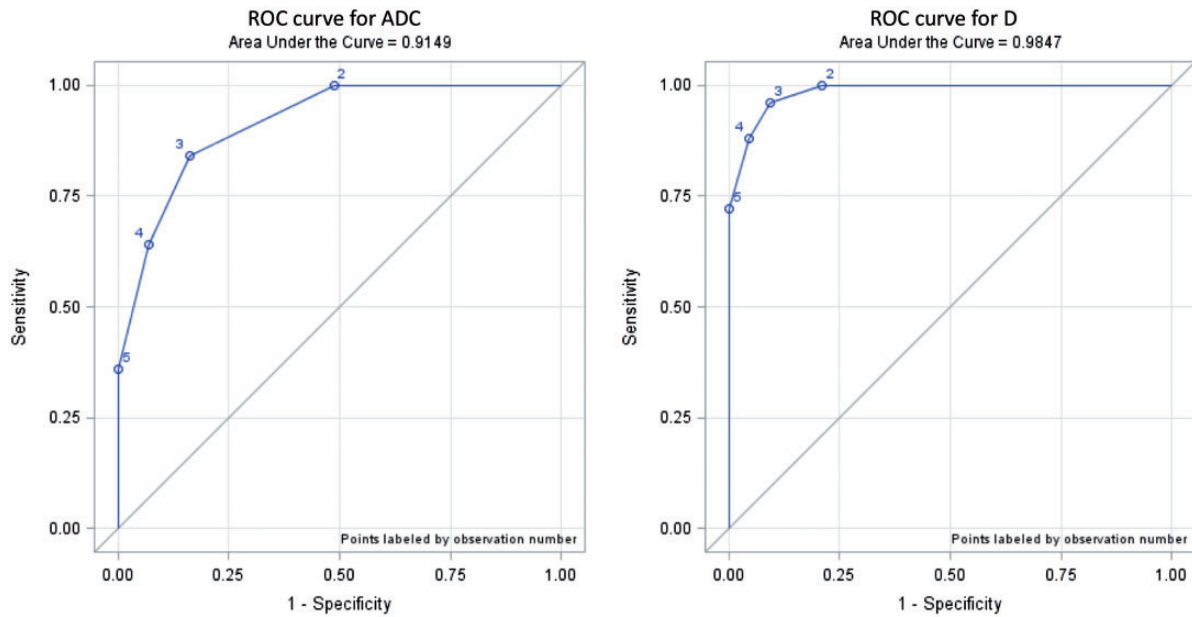


Fig. 3. Receiver operating characteristic (ROC) curve model using ADC (left) and D (right) values and five classes of malignancies (class 1–5) based on ADC and D value limits as summarized in Table 3.

parenchymal micro-perfusion. Thus, DKI might better reveal changes in diffusion restriction, while ADC differences might be attributed to changes in micro-perfusion rather than changes in true diffusion restriction. This is also supported by studies examining intravoxel coherent motion effects in pancreatic DWI (17,18). Additionally, DKI was found to be less influenced by the degree of liver fibrosis (9). Thus, cutoff DKI values for different focal lesion types should be applicable independently of accompanying diffuse liver parenchyma alterations. In their study (9), Goshima et al. found completely necrotic HCC lesions to feature higher ADC but lower mean kurtosis values than viable HCC tissue. This finding implies that several effects—like micro-perfusion—contribute to ADC values, while DKI more likely reveals the differences in true structural complexity. Thus, DKI might also be beneficial in the differentiation and classification of focal liver lesions based on their structural complexity.

Even though recent studies showed that DWI can be acquired before or after contrast media injection with no relevant effect on quantitative ADC values (19), we chose to analyze both groups separately. This was done as the influence of contrast agent administration on DKI values in this setting is not known. Additionally, an influence of the contrast agent was found for both ADC and D for all lesion types in the ANOVA analysis. Thus, before using DKI-based quantitative information in clinical decision-making, further studies on the influence of contrast media administration on those quantitative approaches are necessary.

There are limitations of the present study. The relatively small sample size and the lack of a histological reference for most benign lesions included in our study limit the generalizability of the results herein. Although the accuracy of DKI and DWI was not compared to a histological gold standard in those cases, long-term follow-up was available. Further studies with pathologic correlation as well as DKI imaging with b-values higher than 1000 s/mm^2 are necessary to confirm these initial results and to further investigate the usefulness of DKI for the differentiation of focal liver lesions and its value in comparison to other functional imaging techniques (20).

In conclusion, the application of DKI using a clinical abdominal DWI sequence at 3 Tesla is feasible. Even though the technique allows for accurate discrimination between malignant and benign liver lesions, its additional value compared to conventional ADC values is limited. Further studies including higher b-value DWI will be needed to show the potential benefit of DKI in the differentiation of focal hepatic lesions.

Acknowledgements

The authors thank Lothar Pilz, Department of Biostatistics, Medical Faculty Mannheim, Heidelberg University, for his support in the statistical analyses.

Declaration of conflicting interests

The author(s) declared no potential conflicts of interest with respect to the research, authorship, and/or publication of this article.

Funding

The author(s) received no financial support for the research, authorship, and/or publication of this article.

References

1. Jensen JH, Helpert JA, Ramani A, et al. Diffusional kurtosis imaging: the quantification of non-gaussian water diffusion by means of magnetic resonance imaging. *Magn Reson Med* 2005;53:1432–1440.
2. Jensen JH, Helpert JA. MRI quantification of non-Gaussian water diffusion by kurtosis analysis. *NMR Biomed* 2010;23:698–710.
3. Lu H, Jensen JH, Ramani A, et al. Three-dimensional characterization of non-gaussian water diffusion in humans using diffusion kurtosis imaging. *NMR Biomed* 2006;19:236–247.
4. Jensen JH, Falangola MF, Hu C, et al. Preliminary observations of increased diffusional kurtosis in human brain following recent cerebral infarction. *NMR Biomed* 2011;24:452–457.
5. Raab P, Hattingen E, Franz K, et al. Cerebral gliomas: diffusional kurtosis imaging analysis of microstructural differences. *Radiology* 2010;254:876–881.
6. Wang JJ, Lin WY, Lu CS, et al. Parkinson disease: diagnostic utility of diffusion kurtosis imaging. *Radiology* 2011;261:210–217.
7. Van Cauter S, Veraart J, Sijbers J, et al. Gliomas: diffusion kurtosis MR imaging in grading. *Radiology* 2012;263:492–501.
8. Rosenkrantz AB, Sigmund EE, Johnson G, et al. Prostate cancer: feasibility and preliminary experience of a diffusional kurtosis model for detection and assessment of aggressiveness of peripheral zone cancer. *Radiology* 2012;264:126–135.
9. Goshima S, Kanematsu M, Noda Y, et al. Diffusion kurtosis imaging to assess response to treatment in hypervascular hepatocellular carcinoma. *Am J Roentgenol* 2015;204:W543–549.
10. Rosenkrantz AB, Sigmund EE, Winnick A, et al. Assessment of hepatocellular carcinoma using apparent diffusion coefficient and diffusion kurtosis indices: preliminary experience in fresh liver explants. *Magn Reson Imaging* 2012;30:1534–1540.
11. Kartalis N, Manikis GC, Loizou L, et al. Diffusion-weighted MR imaging of pancreatic cancer: A comparison of mono-exponential, bi-exponential and non-Gaussian kurtosis models. *Eur J Radiol Open* 2016;3:79–85.
12. Weisser G, Sauter E, Zöllner F, et al. UMMDiffusion: Eine OpenSource Software zur klinischen Evaluation der Kurtosis Bildgebung. *Fortschr Röntgenstr, German Congress of Radiology*; 2014. 10.1055/s-0034-1372714.
13. Zöllner F, Kaiser S, Weisser G, et al. UMMDiffusion: An OsiriX plug-in for ADC and IVIM analysis in clinical routine. *Proc Intl Soc Mag Reson Med* 2013;21:3115.
14. Rosenkrantz AB, Padhani AR, Chenevert TL, et al. Body diffusion kurtosis imaging: Basic principles, applications, and considerations for clinical practice. *J Magn Reson Imaging* 2015;42:1190–1202.
15. Glenn GR, Tabesh A, Jensen JH. A simple noise correction scheme for diffusional kurtosis imaging. *Magn Reson Imaging* 2015;33:124–133.
16. Taouli B. Diffusion-weighted MR imaging for liver lesion characterization: a critical look. *Radiology* 2012;262:378–380.
17. Lemke A, Laun FB, Klauss M, et al. Differentiation of pancreas carcinoma from healthy pancreatic tissue using multiple b-values: comparison of apparent diffusion coefficient and intravoxel incoherent motion derived parameters. *Invest Radiol* 2009;44:769–775.
18. Lemke A, Laun FB, Simon D, et al. An in vivo verification of the intravoxel incoherent motion effect in diffusion-weighted imaging of the abdomen. *Magn Reson Med* 2010;64:1580–1585.
19. Cieszanowski A, Podgorska J, Rosiak G, et al. Gd-EOB-DTPA-enhanced MR imaging of the liver: the effect on T2 relaxation times and apparent diffusion coefficient (ADC). *Pol J Radiol* 2016;81:103–109.
20. Malzacher M, Kalayciyan R, Konstandin S, et al. Sodium-23 MRI of whole spine at 3 Tesla using a 5-channel receive-only phased-array and a whole-body transmit resonator. *Z Med Phys* 2016;26:95–100.